

MambaMIM: Pre-training Mamba with State Space Token-interpolation

Fenghe Tang^{1,2†}, Bingkun Nian^{3†}, Yingtai Li^{1,2†}, Jie Yang³, Liu Wei^{3‡}, S. Kevin Zhou^{1,2‡}

¹ School of Biomedical Engineering, Division of Life Sciences and Medicine,
University of Science and Technology of China, Hefei, Anhui, 230026, P.R. China

² Suzhou Institute for Advanced Research,
University of Science and Technology of China, Suzhou, Jiangsu, 215123, P.R. China

³ Department of Automation, Institute of Image Processing and Pattern Recognition,
Shanghai Jiao Tong University, Shanghai, China

Abstract

Generative self-supervised learning demonstrates outstanding representation learning capabilities in both Convolutional Neural Networks (CNNs) and Vision Transformers (ViTs). However, there are currently no generative pre-training methods related to selective state space models (Mamba) that can handle long-range dependencies effectively. To address this challenge, we introduce a generative self-supervised learning method for Mamba (**MambaMIM**) based on Selective Structure State Space Sequence Token-interpolation (S6T), a general-purpose pre-training method for arbitrary Mamba architectures. Our method, MambaMIM, incorporates a bottom-up 3D hybrid masking strategy in the encoder to maintain masking consistency across different architectures. Additionally, S6T is employed to learn causal relationships between the masked sequence in the state space. MambaMIM can be used on any single or hybrid Mamba architectures to enhance the Mamba long-range representation capability. Extensive downstream experiments reveal the feasibility and advancement of using Mamba for pre-training medical image tasks. The code is available at: <https://github.com/FengheTan9/MambaMIM>.

1 Introduction

Recently, state space models demonstrate their efficiency and effectiveness in long sequence modeling (Gu, Goel, and Ré 2021). Especially its variant Mamba (Gu and Dao 2023; Dao and Gu 2024), enhanced by selective scan and hardware aware implementation, demonstrates competitive performance against Transformer (Vaswani et al. 2017) across both natural language (Vaswani et al. 2017) and DNA sequence modeling (Zhou et al. 2024). For computer vision tasks, Vision Mamba (Zhu et al. 2024) emerges as a potential solution to long-range dependency modeling for image, achieving promising performance across a wide range of vision tasks (Liu, Zhang, and Zhang 2024). Transitioning from broader computer vision applications to medical image analysis (MIA), Vision Mamba also offers competitive performance (Ma, Li, and Wang 2024; Xing et al. 2024; Liu et al. 2024). However, due to the scarcity of labeled data in MIA and the inherent properties of state space sequences, training

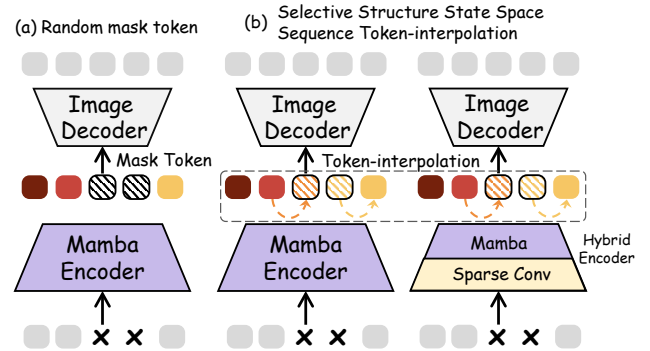


Figure 1: Different token generation strategies for Mamba-based network. (a) Random learnable mask token for decoding which ignores structure sequence relationships within the state space. (b) Straightforward idea to apply causality of selective state space sequences for arbitrary Mamba.

high performance vanilla Vision Mamba for medical downstream tasks is demanding (Ruan and Xiang 2024). Hybrid architectures (Wenxuan et al. 2021; Chen et al. 2021; Tang et al. 2023; Ma, Li, and Wang 2024; Xing et al. 2024) can utilize inductive bias of convolution (Ronneberger, Fischer, and Brox 2015) to compensate for the lack of local feature extraction capabilities, but it still struggles to further breakthrough performance.

Fortunately, self-supervised learning provides a promising approach for MIA (Zhang, Zheng, and Gu 2023), which first pre-trains a model on a large corpus of easily-collected unlabeled images and then transfers it to downstream tasks (Tang et al. 2022; Zhou et al. 2019; Goncharov et al. 2023). Such a pretrain-finetune paradigm can greatly boost the performance in data-scarce downstream tasks. Most successful self-supervised learning methods for vision tasks are contrastive-based (Chen et al. 2020; He et al. 2020; Grill et al. 2020; Caron et al. 2020; Chen and He 2021; Caron et al. 2021) and generative-based (Devlin et al. 2018; Pathak et al. 2016; Bao et al. 2021; Zhou et al. 2021; He et al. 2022; Xie et al. 2022; Assran et al. 2023; Chen et al. 2024; Tian et al. 2023). Among them, generative-based methods, represented by a series of masked image modeling (MIM) approaches, exhibit a stronger transfer ability (He

[†] These authors contributed equally. [‡] Corresponding Author

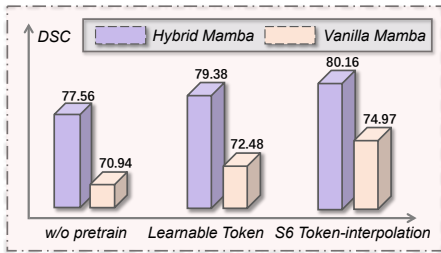


Figure 2: Vanilla Mamba v.s. Hybrid Mamba with different mask token strategies pre-trained on the BTCV dataset (Landman et al. 2015) for the 3D segmentation task. vanilla Mamba: Vision Mamba replaces ViT in UNETR (Hatamizadeh et al. 2022); hybrid Mamba (HyMamba): MedNeXt (Roy et al. 2023) (CNN) + Mamba. The improvements brought by S6T surpass previous SSL-methods with the learnable token, and they are much better than those without pre-training.

et al. 2022; Xie et al. 2022; Assran et al. 2023; Chen et al. 2024; Tian et al. 2023). However, MIM methods require handling masked and seen patches, which usually involves strategies tailored for a certain architecture (Xie et al. 2022; He et al. 2022; Tian et al. 2023), making existing MIM insufficient when applied to Vision Mamba models.

How to pretrain Vision Mamba models in a generative style remains a scientifically meritorious yet unrealized topic because of the difficulty in modeling from 3D spatial volume to state space sequences. As shown in Fig.1(a), for masking strategy in pre-training Mamba with MIM, one straightforward idea could involve dropping masked patches and inserting learnable tokens at masked positions to reconstruct masked pixels, a technique previously employed in MAE (He et al. 2022) for ViTs (Dosovitskiy et al. 2020). However, our preliminary experiments indicate that while learnable tokens have some effect on vanilla Mamba and hybrid Mamba, its performance is not yet satisfactory (shown in Fig. 2). We attribute this shortcoming to *the insertion of learnable tokens that does not comply with the causal and input-dependent selective scan property*. Since these tokens ignore structure sequence relationships within a state space, the historical information is unfortunately selected by randomly initialized learnable tokens and may fail to be effectively conveyed to subsequent tokens. Although the hybrid architecture of CNN-Mamba can relatively improve performance, the aforementioned issues still persist. Furthermore, for CNN-Mamba hybrid models, maintaining a masking consistency between the convolution and Mamba layers is critical for end-to-end training. *An inconsistent masking across different architectures could result in pixel distribution shifts*, negatively impacting representation learning (Tian et al. 2023).

To solve the above challenge, we propose a Mamba-specific masking modeling strategy named MambaMIM for pretraining CNN-Mamba hybrid models with large-scale 3D CT datasets. As a pretraining model, MambaMIM can use a distinctive token generation method called selective structure state space sequence token-interpolation (S6T) shown

in Fig.1(b), which allows to effectively utilize the relationships between structure state space sequences in the Mamba model for token generation. Moreover, in the encoder, we maintain mask consistency through bottom-up mask modeling to keep end-to-end CNN-Mamba pre-training.

It is noteworthy that MambaMIM is not restricted to pre-training on hybrid architectures. It can also be used to pre-train vanilla Vision Mamba models (special case in hybrid models) which can be seen in Fig. 2. Through our proposed MambaMIM, we successfully enable generative-based pre-training to benefit both vanilla Mamba and hybrid Mamba architectures. To the best of our knowledge, MambaMIM is the first self-supervised pre-training method specifically designed for Mamba and selective structure state space sequence. Across multiple medical image segmentation tasks, the CNN-Mamba hybrid model pre-trained with MambaMIM outperforms other state-of-the-art self-supervised pre-training methods and architectures. Our contributions are summarized as follows:

- We propose MambaMIM, a generative self-supervised learning method for pre-training CNN-Mamba hybrid architectures that can learn local and global representations. To the best of our knowledge, MambaMIM is the first attempt to explore the potential of vanilla Vision Mamba and hybrid Mamba in pre-training tasks.
- We propose a novel token generation method called selective structure state space sequence token-interpolation (S6T) for Mamba during decoding, which prioritizes consistency across the state space and maximizes the potential of Mamba for representation learning.
- We pre-train a strong hybrid vision encoder using MambaMIM on large-scale 3D CT datasets and fine-tune on downstream tasks. Extensive experiments demonstrate the effectiveness and potential of MambaMIM with state-of-the-art performance achieved.

2 Methodology

In order to utilize our pre-training method MambaMIM, a CNN-Mamba hybrid model called HyMamba (CNN on the top and Vision Mamba at the bottom) is selected as the baseline backbone. The hybrid model leverages Mamba after the final stage of CNN to enhance long-range dependency.

2.1 Hierarchical Hybrid Encoding

To achieve end-to-end pretraining of the hierarchical CNN-Mamba hybrid model while maintaining a mask consistency between the CNN stage and the Mamba stage of the encoder, as shown in Algorithm 1, a hybrid masking strategy in a bottom-up manner is implemented. Specifically, given the input volume $X \in \mathbb{R}^{H \times W \times D}$, we initialize the mask $M_n \in \mathbb{R}^{\frac{H}{n^2} \times \frac{W}{n^2} \times \frac{D}{n^2}}$ at the n -th CNN stage. Then, we map the initialized mask M_n to other CNN stages and generate a set of masks $\{M_1, M_2, \dots, M_{n-1}\}$ by patch upsampling at different scales in the same manner. For the CNN stage of the hybrid model, following previous work (Tian et al. 2023; Woo et al. 2023), we introduce 3D sparse operator (SparseOp) to skip compute the masked positions and

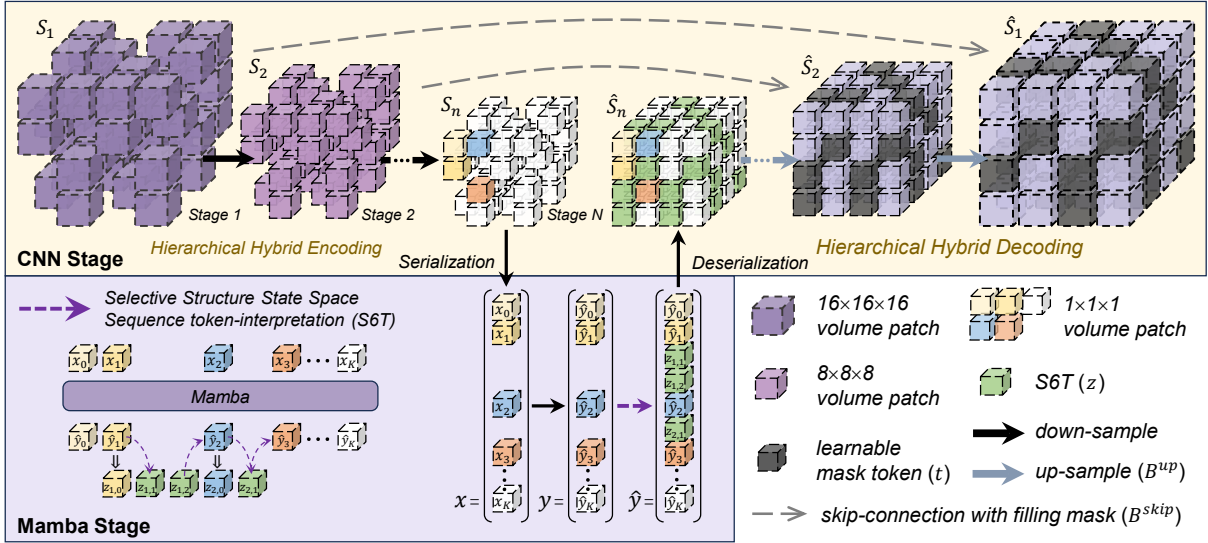


Figure 3: The whole structure of MambaMIM. The hybrid encoder performs bottom-up masked modeling, the initialization unmasking patch is white, the bottom-up mapping unmasking patch is purple and the masking position is empty. The CNN stage (yellow) utilizes 3D sparse operator for hierarchical encoding and fill learnable mask token in masked position for decoding. The Mamba stage (purple) only learns unmasked sequence, and S6T is applied during decoding which can preserve the continuity of 1D selective structure state space sequence.

Algorithm 1: Hierarchical Hybrid Encoding

Input: Image volume X
Output: a set of sparse features $\{y, S_{n-1}, \dots, S_2, S_1\}$
Initialize: random masking M_n

- 1: $\{M_{n-1}, M_{n-2}, \dots, M_2, M_1\} \leftarrow M_n$
- 2: $S_1 \leftarrow \text{SparseOp}(X, M_1)$
- 3: **for** $i = 2$ **to** n **do**
- 4: $S_i \leftarrow \text{SparseOp}(S_{i-1}, M_i)$
- 5: **end for**
- 6: $x \leftarrow \text{Serialization}(S_n, M_n)$
- 7: $y \leftarrow \text{Mamba}(x)$
- 8: **return** $\{y, S_{n-1}, \dots, S_2, S_1\}$

generate different scale sparse features $\{S_1, S_2, \dots, S_n\}$. As for the Mamba stage, the sparse feature S_n is serialized and we discard the masked sequence, and only calculate the unmasked tokens x for generating unmask state space sequence y . Note that, the final output of the encoder is hierarchical sparse features $\{S_1, S_2, \dots, S_{n-1}, y\}$ under the same masking strategy. The detailed encoding process is in Algorithm 1.

2.2 Hierarchical Hybrid Decoding.

We introduce a simple cascaded decoder comprising $N-1$ upsampling blocks $\{B_1^{up}, B_2^{up}, \dots, B_{n-1}^{up}\}$ and skip-connection blocks $\{B_1^{skip}, B_2^{skip}, \dots, B_{n-1}^{skip}\}$ for upstream to downstream alignment and hierarchical dense reconstruction, which is shown in Algorithm 2. Before decoding, it is necessary to implement different mask filling strategies according to the characteristic of each architecture. Specif-

Algorithm 2: Hierarchical Hybrid Decoding

Input: a set of sparse features $\{y, S_{n-1}, \dots, S_2, S_1\}$
Output: reconstruction map \hat{X}

- 1: $\hat{y} \leftarrow \text{S6T}(y)$
- 2: $D_n \leftarrow \phi(\hat{y})$
- 3: **for** $i = n - 1$ **to** 1 **do**
- 4: $\hat{S}_i \leftarrow \text{Fill}(S_i, t_i)$
- 5: $D_i \leftarrow B_i^{skip}(\text{Concat}\{\phi(\hat{S}_i), B_i^{up}(D_{i+1})\})$
- 6: **end for**
- 7: $\hat{X} \leftarrow \tau(D_1)$
- 8: **return** \hat{X}

ically, for the Mamba stage, a novel state space interpolation called selective structured state space sequence token-interpolation (S6T) is proposed to preserve the continuity of 1D selective structure state space sequences (in Sec. 2.3). As for the CNN stage, we fill learnable token embeddings $\{t_{n-1}, \dots, t_2, t_1\}$ into all empty positions of 3D sparse features $\{S_1, S_2, \dots, S_{n-1}\}$ at different scales to get dense features $\{\hat{S}_1, \hat{S}_2, \dots, \hat{S}_{n-1}\}$. And operation projection ϕ is used to reduce the width of dense features. With the skip connections of dense features, the network could learn multi-scale representations better. Finally, we utilize a linear layer τ to get reconstruct map \hat{X} . The detailed decoding process is presented in Algorithm 2.

2.3 Selective Structured State Space Sequence Token-interpolation

Different from other MIM methods like MAE (He et al. 2022) which simply inserts learnable tokens at masked po-

sition to reconstruct masked pixels, S6T can further leverage the causation of the structure sequence for selective state space token-interpolation to improve the representation capabilities of the encoder. Unlike ViT or CNN, Mamba predicts hidden states rather than simply aggregating semantic information, which means that masked positions cannot be simply filled with random mask tokens.

Analysis and Problems. In modern state-space models, structured state space sequence models (S4) and Mamba both rely on a classical continuous system that maps one-dimensional input function or sequence, denoted as $x(t) \in \mathcal{R}$, through inter-mediate implicit state $h(t) \in \mathcal{R}^N$ to an output $y(t) \in \mathcal{R}$. The whole process can be represented as a linear Ordinary Differential Equation (ODE):

$$\begin{aligned} h'(t) &= Ah(t) + Bx(t), \\ y(t) &= Ch(t), \end{aligned} \quad (1)$$

where $A \in \mathcal{R}^{N \times N}$ means the state matrix like combination coefficient, $B \in \mathcal{R}^{N \times 1}$ and $C \in \mathcal{R}^{N \times 1}$ represents computation parameters. To make it more suitable for deep learning scenarios, discretization is performed. A timescale parameter Δ is utilized. And \bar{A} and \bar{B} with zero-order hold can be defined as follows:

$$\begin{aligned} \bar{A} &= \exp(\Delta A), \\ \bar{B} &= (\Delta A)^{-1}(\exp(\Delta A) - I) \cdot \Delta B. \end{aligned} \quad (2)$$

After discretization, SSM-based models can be computed in following way: global convolution, defined as Equ. 13:

$$\begin{aligned} \bar{K} &= (C\bar{B}, C\bar{A}\bar{B}, \dots, C\bar{A}^{L-1}\bar{B}), \\ y &= x * \bar{K}, \end{aligned} \quad (3)$$

where $\bar{K} \in \mathcal{R}^L$ represents a structure convolutional kernel, and L is the length of the input sequence x .

To facilitate theoretical deduction, we express Equ. 13 as a series of summations.

$$\begin{aligned} y &= (y_0, y_1, \dots, y_j, \dots, y_L), \\ y_j &= \sum_{i=0}^j C \cdot \bar{A}^{j-i} \cdot \bar{B}x_i. \end{aligned} \quad (4)$$

Taking masked image modeling into consideration, Ω represents the masked sequence index. Define $\Gamma_\Omega(i)$ as the querying the index of the i -th element of y in the sequence Ω and Equ. 4 can be further expressed via:

$$\begin{aligned} \hat{y} &= (\hat{y}_0, \hat{y}_1, \dots, \hat{y}_L), \\ \hat{y}_i &= \begin{cases} \sum_{n=0}^j C \cdot \bar{A}^{j-n} \cdot \bar{B}x_j, j = \Gamma_\Omega(i), \text{ if } i \in \Omega \\ \delta, \text{ if } i \in \bar{\Omega} \end{cases}, \end{aligned} \quad (5)$$

where δ represents learnable parameters, which are often set to identity matrix. It can be seen that δ helps the encoder to learn sparse semantic information, but it has a possibility of failure for the intrinsic relationships of the structure state space. The success of Mamba on vision task relies on exploration of inter-mediate implicit states. Simply filling

Algorithm 3: selective structure state space sequence token-interpretation (S6T)

Input: $y = [\hat{y}_i, \hat{y}_{i+1}], Q + 1$,

Parameter: Learnable Parameters \bar{A}'

Operator: Exponentiation $\text{Pow}(\cdot)$

Output: S6T sequence \hat{y}

```

1: for  $j = 1$  to  $Q + 1$  do
2:    $\alpha \leftarrow \frac{j}{Q+2}$ 
3:    $V \leftarrow (1 - \alpha) \cdot \hat{y}_i + \alpha \cdot \hat{y}_{i+1}$ 
4:    $z_j \leftarrow \sum_{n=0}^j \text{Pow}(A', j - n) \Delta A'^{-1} \cdot V$ 
5: return  $\hat{y} \leftarrow [\hat{y}_i = z_0, z_1, z_2, \dots, z_{Q+1}]$ 

```

masked sequence with tokens δ may not satisfy this mathematical relation and not suitable for Mamba. *In order to enable filled sequences to meet with causal relationships in structure state space, S6T is proposed.*

Equation of S6T. We fill sequence and it can be rearranged into the following form. Given the masked input sequence $x = (x_0, \dots, x_K)$, masked Mamba sequence $y = (\hat{y}_0, \dots, \hat{y}_K)$ is achieved after Mamba block. We present a generalizable masked decoding scenario:

$$\begin{aligned} \hat{y} &= (\hat{y}_0, \dots, \hat{y}_i, z_0, z_1, \dots, z_Q, \hat{y}_{i+1}, \hat{y}_{i+2}, \dots, \hat{y}_K), \\ T &= Q + K + 2, \\ \hat{y}_j &= \sum_{n=0}^j C \cdot \bar{A}^{j-n} \cdot \bar{B}s_n, \\ z_i &= \delta, \end{aligned} \quad (6)$$

where \hat{y} is the decoding sequence, $K + 1$ is the number of the unmasked token in Mamba sequence, $Q + 1$ is the number of the filled tokens and T is the length of the whole reconstruction sequences. We hypothesize that if the position of z_i is left unfilled by a token, the entire sequence forms a complete selective state space. To restore this deductive relationship, we assume that the sequence $(\hat{y}_i, z_0, z_1, \dots, z_Q, \hat{y}_{i+1})$ also satisfies this relationship. This can be represented as:

$$\begin{aligned} \hat{y}_i &= C' \bar{B}' s'_0, \\ z_i &= \sum_{n=0}^i C' \cdot \bar{A}'^{i-n} \cdot \bar{B}' s'_n, \\ \hat{y}_{i+1} &= \sum_{n=0}^{Q+2} C' \cdot \bar{A}'^{Q+2-n} \cdot \bar{B}' s'_n, \\ s'_n &= \frac{Q+2-n}{Q+2} \cdot \hat{y}_i + \frac{n}{Q+2} \cdot \hat{y}_{i+1}, \end{aligned} \quad (7)$$

where C' , \bar{B}' , \bar{A}' can be set as learnable parameters, and theoretically, all the values are solvable. However, obtaining these values is challenging for the network. We observe that if we set A' as learnable parameters, the effects of C' and B' could be represented by A' via gradient update. For simplification, let $B' = C' = E$ (identity matrix). Then \bar{B}' can be written as $(e^{\Delta A'} \Delta A'^{-1} - \Delta A'^{-1}) \approx e^{\Delta A'} \Delta A'^{-1}$.

Network	Pre-training	Spl	Kid	Gall	Eso	Liv	Sto	Aor	IVC	Veins	Pan	AG	Avg
UNETR	\times	86.14	82.73	55.99	67.23	92.50	73.80	85.26	77.59	59.81	53.71	53.75	71.15
Swin UNETR	\times	88.51	81.85	58.39	71.72	94.18	78.47	86.97	80.51	66.96	64.71	60.13	74.95
MedNeXt	\times	89.27	83.88	60.85	71.66	94.30	79.39	88.94	82.25	64.85	70.63	59.94	76.14
SegMamba	\times	88.19	82.11	61.52	70.54	93.29	80.13	87.24	82.81	66.31	72.38	64.23	76.54
3D U-Net (FPN)	\times	88.77	80.54	61.76	74.40	94.88	80.93	88.25	83.21	67.68	71.92	62.22	76.72
vanilla Mamba	\times	85.08	82.61	58.65	68.25	92.66	72.35	84.12	75.94	56.68	53.34	52.96	70.94
	\checkmark (MambaMIM)	86.78	84.85	62.68	69.58	92.94	79.45	87.66	79.99	61.88	65.30	59.40	74.97
HyMamba	\times	88.60	87.18	60.67	74.73	94.34	79.60	88.67	82.07	68.83	71.53	62.43	77.56
	\checkmark (MambaMIM)	89.67	87.23	65.93	73.91	95.00	86.20	91.08	84.26	70.40	79.11	64.81	80.16

Table 1: Results of the baseline backbone on BTCV for the 3D segmentation task. **val** (bold) / val (underline) : top method / second method. HyMamba: baseline backbone of MambaMIM which consists of hybrid MedNeXt and Vision Mamba.

It is worth noting that this system of equations is derived from a new state-space equation, where \bar{B}' is further expressed and eliminated by \bar{A}' , rather than directly removed. Moreover, the meaning of A' also differs slightly from that in the original Mamba theory. For the detailed derivation process, *please refer to the supplementary materials*. Through this simplification, we could obtain a more concise expression:

$$\begin{aligned}
z_i &= \sum_{n=0}^i (\bar{A}'^{i-n} \Delta A'^{-1}) \cdot s'_n, \\
s'_n &= \frac{Q+2-n}{Q+2} \cdot \hat{y}_i + \frac{n}{Q+2} \cdot \hat{y}_{i+1}, \\
\bar{A}' &= e^{\Delta A'}.
\end{aligned} \tag{8}$$

We call z_i as selective structured state space sequence token-interpretation (S6T) and S6T is presented in Algorithm. 3. S6T is only used during the pre-training to perform the sparse image reconstruction task (the encoder is used for downstream tasks). Therefore, the decoder architecture can be flexibly designed, independent of the encoder design.

3 Experiment

3.1 Dataset

Pre-training datasets. A total of 13 public CT datasets, consisting of 6,814 CT scans, are curated to form our pre-training dataset. Existing labels are not utilized from these datasets during the pre-training stage. The pre-training data are interpolated to isotropic voxel spacing of 1.5 mm. Intensities are scaled to $[-175, 250]$ and then normalized to $[0, 1]$. We crop sub-volumes of $96 \times 96 \times 96$ voxels.

BTCV dataset. The Multi-Atlas Labeling Beyond The Cranial Vault (BTCV) (Landman et al. 2015) dataset consists of 30 subjects with abdominal CT scans where 13 organs are annotated at pixel level by interpreters under the supervision of clinical radiologists at Vanderbilt University Medical Center. Our data preprocessing strategy is the same as UNETR (Hatamizadeh et al. 2022).

MSD dataset. Medical Segmentation Decathlon (MSD) dataset (Antonelli et al. 2022) comprises of ten segmentation tasks from different organs and image modalities. We only use three CT datasets: Pancreas, Hepatic Vessel, Spleen dataset. All the pre-processing strategy is the same as Swin UNETR (Tang et al. 2022).

3.2 Implementation details

Components. MambaMIM can be utilized to vanilla Mamba or hybrid Mamba comprised of any convolution network and Mamba. We perform separate pre-training for the encoder and the decoder. And the encoder is fine-tuned for downstream medical segmentation task.

Implementation of pre-training. For the pre-training of the medical reconstruction task, we train the network with an AdamW optimizer, a learning rate of $1e-4$ and a cosine-annealing learning rate scheduler. The batch size is set to 8, and the model is trained for 100 epochs on a single GPU. For downstream segmentation tasks, a five-fold cross validation strategy is used to train models for all BTCV and MSD experiments and the best model is selected on each fold. Detailed training hyperparameters for fine-tuning BTCV and MSD tasks are the same as that of Swin UNETR (Tang et al. 2022). All methods are implemented in PyTorch and trained on an Nvidia A800 GPU.

Loss function. During the pre-training, given the output prediction of reconstruction \hat{X} and input volume X , a mean square error loss (\mathcal{L}_2) is used for the reconstruction optimization of normalized pixels at masked positions. During fine-tuning, we use a combined loss ($\mathcal{L}_{seg} = \mathcal{L}_{BCE} + \mathcal{L}_{DSC}$) of binary cross entropy loss (\mathcal{L}_{BCE}) and DSC loss (\mathcal{L}_{DSC}) to optimize the network.

Evaluation metrics and comparison methods. The DSC similarity coefficient (DSC) metric is used as measurements for all experimental results (Lay et al. 2013) on BTCV and MSD. We select three advanced generative-based self-supervised learning strategies: Transformer-based MAE (He et al. 2022) and SimMIM (Xie et al. 2022), CNN-based SparK (Tian et al. 2023), three advanced contrastive-based self-supervised learning methods: SimSiam (Chen and He 2021), SwAV (Caron et al. 2020), MoCoV2 (He et al. 2020), vox2vec (Goncharov et al. 2023) and a hybrid pre-training objective used in Swin UNETR Pretrain method (SUP) (Tang et al. 2022). In addition, we choose the current well-known segmentation networks UNETR (Hatamizadeh et al. 2022), Swin UNETR (Tang et al. 2022), MedNeXt (Roy et al. 2023), 3D U-Net (FPN) (Goncharov et al. 2023), vanilla Mamba (Gu and Dao 2023) and SegMamba (Xing et al. 2024) for segmentation.

Pre-training method		Spl	Kid	Gall	Eso	Liv	Sto	Aor	IVC	Veins	Pan	AG	Avg(%)
Method	Backbone												
MoCov2 [†]	HyMamba	88.72	82.63	65.00	73.26	93.48	76.09	85.53	79.92	66.93	63.09	59.55	75.11
SimSiam [†]	HyMamba	88.50	85.46	65.31	75.22	94.15	77.35	88.66	82.12	68.88	71.65	62.20	77.48
SUP ^{†‡}	HyMamba	88.52	84.06	68.45	73.36	93.82	<u>80.78</u>	<u>89.52</u>	81.89	66.81	69.54	<u>63.42</u>	77.83
SwAV [†]	HyMamba	89.78	88.35	65.38	<u>74.40</u>	<u>94.54</u>	79.29	88.42	<u>82.23</u>	<u>69.96</u>	<u>73.11</u>	61.91	<u>78.28</u>
MambaMIM [‡]	HyMamba	<u>89.67</u>	<u>87.23</u>	65.93	73.91	95.00	86.20	91.08	84.26	70.40	79.11	64.81	80.16

Table 2: Comparison between MambaMIM and other pre-training methods with the same baseline model on BTCV for the 3D segmentation task. **val** (bold) / val (underline) : top method / second method. †: Contrastive-based method. ‡: Generative-based method.

Pre-training method		MSD Pancreas			MSD Hepatic Vessel			MSD Spleen	BTCV					Avg(%)	
Method	Network	DSC1	DSC2	Avg(%)	DSC1	DSC2	Avg(%)	DSC	Gall	Sto	IVC	Pan	AG		Avg(%)
vox2vec [†]	3D UNet (FPN)	77.00	31.80	54.40	59.50	62.40	60.95	96.10	59.50	83.20	<u>83.90</u>	73.90	65.20	<u>79.50</u>	72.73
SUP ^{†‡}	Swin UNETR	75.20	35.90	55.55	60.90	57.50	59.20	95.50	68.45	80.78	81.89	69.54	63.42	77.83	72.02
MAE [‡]	UNETR	77.76	39.29	58.52	59.99	62.22	61.10	95.28	62.50	<u>86.11</u>	83.26	75.47	63.77	79.07	73.49
SimMIM [‡]	Swin UNETR	76.16	44.96	60.56	60.67	61.79	61.23	95.64	60.28	78.42	81.46	66.34	58.65	74.73	73.04
SparK [‡]	MedNeXt	<u>78.88</u>	<u>47.86</u>	<u>63.37</u>	<u>61.08</u>	<u>67.76</u>	<u>64.42</u>	<u>96.18</u>	62.48	84.85	83.60	<u>76.57</u>	64.13	79.21	<u>75.79</u>
MambaMIM [‡]	HyMamba	78.90	51.01	64.96	61.61	68.22	64.91	96.41	<u>65.93</u>	86.20	84.26	79.11	64.81	80.16	76.61

Table 3: Performance of other state-of-the-art pre-training methods on BTCV and MSD for the 3D segmentation task. **val** (bold) / val (underline) : top method / second method. †: Contrastive-based method. ‡: Generative-based method.

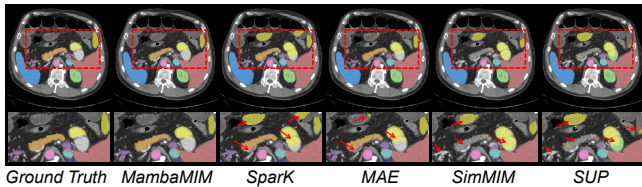


Figure 4: Visualization results on BTCV dataset.

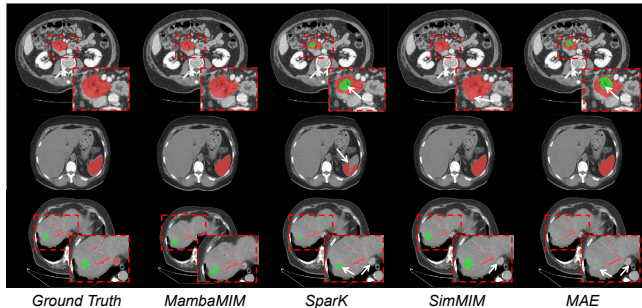


Figure 5: Visualization results on MSD datasets.

3.3 Results and discussion

Performance of MambaMIM. We first validate the proposed method MambaMIM and its baseline model on BTCV. The results are listed in Table. 1. HyMamba achieves the highest average metric of 77.56% when trained from scratch, surpassing Mamba by 6.62% (77.56% vs. 70.94%) and SegMamba by 1.02% (77.56% vs. 76.54%). This shows that the hybrid architecture can maximize the long-range extraction capability of Mamba, which is crucial for medical image segmentation tasks. More importantly, our core contribution lies in MambaMIM, which gains a huge leap in DSC score (2.6% improvement, 80.16% vs 77.56%). For

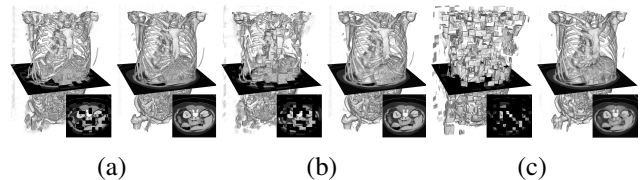


Figure 6: Reconstruction results by MambaMIM with different mask ratios (left: masked input, right: reconstruction result): (a) mask 25% (b) mask 50% (c) mask 75%.

organs that are small in scale and challenging to segment, such as gallbladder (Gall: 5.26% improvement), stomach (Sto: 6.60% improvement), pancreas (Pan: 7.58% improvement), etc., the performance gains are more pronounced, which demonstrates that MambaMIM effectively learns both local and global representations.

Since different networks have different optimal pre-training methods, we selected the method with the best pre-training performance for each network shown in Table. 3. Our proposed MambaMIM outperforms other pre-training methods, which achieves at least 1.59% (64.96% vs 63.37%), 0.49% (64.91% vs 64.42%) and 0.23% (96.41% vs 96.18%) improvements in MSD Pancreas, MSD Hepatic Vessel and MSD Spleen respectively. For lesion segmentation across different datasets, MambaMIM achieves improvements of at least 3.15% in Pancreas and 0.46% in Hepatic Vessel, due to our proposed S6T. S6T further enhances Mamba’s global localization capability. When combined with CNNs, it achieves a highly competitive performance gains of 0.95% in multi-organ segmentation task (shown in Fig. 4). It is worth noting that MambaMIM also enables precise lesion segmentation (shown in Fig. 5). This shows that MambaMIM indeed helps hybrid network effectively to learn strong multi-scale representations.

Mask Ratio	Spl	Kid	Gall	Eso	Liv	Sto	Aor	IVC	Veins	Pan	AG	BTCV Avg(%)
w/o pretrained	88.60	87.18	60.67	<u>74.73</u>	94.34	79.60	88.67	82.07	68.83	71.53	62.43	77.56
mask 25 %	89.18	87.75	63.93	74.92	<u>94.81</u>	83.99	89.71	83.40	69.42	<u>77.26</u>	64.48	79.31
mask 50 %	90.75	<u>87.72</u>	<u>64.06</u>	74.76	94.63	<u>84.17</u>	<u>90.54</u>	<u>84.25</u>	72.01	75.30	65.60	<u>79.78</u>
mask 75 %	<u>90.47</u>	88.06	65.93	73.91	95.00	86.20	91.08	84.26	<u>70.40</u>	79.11	64.82	80.16

Table 4: Ablation study on mask ratio for the BTCV 3D segmentation task. val (bold) / val (underline): top method / second method. **val** (bold) / val (underline) : top method / second method.

MambaMIM components	Hybrid MIM	Skip -connection	State Space Interpolation	BTCV Avg(%)
w/o pretrained	—	—	—	77.56
w/o bottom-up masking	✗	✗	✗	79.20
w/o skip	✓	✗	✗	79.25
w/o state space interpolation	✓	✓	✗	79.38
MambaMIM	✓	✓	✓	80.16

Table 5: Ablation on each component in MambaMIM. The experiment is performed on BTCV for the 3D segmentation task.

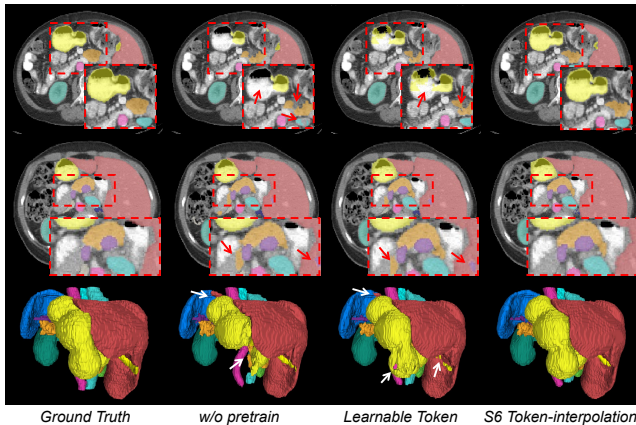


Figure 7: Visualization of ablative results on BTCV dataset.

Performance of different pre-training methods on the baseline model. We also validate different pre-training methods on BTCV under the same base backbone HyMamba. The average DSC score on the BTCV datasets for all contrastive-based pre-training methods are presented in Table. 2. MambaMIM performs much better than other self-supervised methods, which improve the segmentation performance by at least 1.88%. It is also shown that the generative-based methods can gain better transferring than contrastive-based method in segmentation tasks.

Visualization. We visualize 3D reconstruction results with different mask ratios to show what MambamMIM learns in the pre-training. As shown in Fig. 6, our method can almost reconstruct the different shapes of organs, bones, and other details from the different portion of unmasked patches.

3.4 Ablation study

Ablation Study on the Mask Ratio. Table. 4 shows the impact of different mask ratios on the model’s performance. A relatively small 25% mask ratio substantially boosts the performance from 77.56% to 79.31%, indicating that even a

small amount of masking significantly enhances the performance, which demonstrates the effectiveness of generative pre-training. Increasing the mask ratio results in a consistent performance improvement.

Ablation on MambaMIM Components. Table. 5 explores the effects of omitting various components of the MambaMIM framework. Removing the bottom-up masking leads to a performance drop, showing that bottom-up masking contributes to the model’s performance. Although the upper CNN accounts for the majority of the hybrid model’s performance, pre-training still greatly boosts the performance without a consistent mask. Nevertheless, our bottom-up masking strategy still further lifts the performance. Incorporating skip-connection in pre-training improves the performance from 79.25% to 79.38%, which demonstrates the importance of upstream and downstream pattern alignment. Utilizing our proposed S6T greatly enhances the performance from 79.38% to 80.16%, highlighting the effectiveness of state-space interpolation in Mamba pre-training. Additionally, we visualize the segmentation results under different ablation components. As in the Fig. 7, our initiative demonstrates significant benefits for downstream tasks.

4 Limitations

Our proposed MambaMIM is only tried on CT scans and not applied to other modalities. Its generalizability to other imaging modalities (e.g. MRI, Ultrasound) has not been thoroughly evaluated. Different modalities may present unique challenges that could affect the performance and applicability of the MambaMIM approach. We believe that cross-domain MambaMIM, such as pre-training on large-scale CT and performing downstream tasks on completely different datasets (e.g. MRI), still needs to be explored.

5 Conclusion

The success of Mamba in vision tasks prompts us to explore their potential in downstream tasks after being well pre-trained using large-scale unlabeled medical images. In this paper, we introduce MambaMIM, a novel generative self-supervised method based on selective structure state space sequence token-interpolation for single and hybrid Mamba architectures pre-training. Our method uses a bottom-up masking strategy to guarantee the consistency of masked region between CNN and Mamba. Additionally, S6T is employed to learn causal relationships between the masked sequence in the state space. We believe that MambaMIM can further benefit our community and our findings can inspire more work to maximize the potential of Mamba in various visual tasks.

References

- Antonelli, M.; Reinke, A.; Bakas, S.; Farahani, K.; Kopp-Schneider, A.; Landman, B. A.; Litjens, G.; Menze, B.; Ronneberger, O.; Summers, R. M.; et al. 2022. The medical segmentation decathlon. *Nature communications*, 13(1): 4128.
- Assran, M.; Duval, Q.; Misra, I.; Bojanowski, P.; Vincent, P.; Rabbat, M.; LeCun, Y.; and Ballas, N. 2023. Self-supervised learning from images with a joint-embedding predictive architecture. In *Proceedings of the IEEE/CVF Conference on Computer Vision and Pattern Recognition*, 15619–15629.
- Bao, H.; Dong, L.; Piao, S.; and Wei, F. 2021. Beit: Bert pre-training of image transformers. *arXiv preprint arXiv:2106.08254*.
- Caron, M.; Misra, I.; Mairal, J.; Goyal, P.; Bojanowski, P.; and Joulin, A. 2020. Unsupervised learning of visual features by contrasting cluster assignments. *Advances in neural information processing systems*, 33: 9912–9924.
- Caron, M.; Touvron, H.; Misra, I.; Jégou, H.; Mairal, J.; Bojanowski, P.; and Joulin, A. 2021. Emerging properties in self-supervised vision transformers. In *Proceedings of the IEEE/CVF international conference on computer vision*, 9650–9660.
- Chen, J.; Lu, Y.; Yu, Q.; Luo, X.; Adeli, E.; Wang, Y.; Lu, L.; Yuille, A. L.; and Zhou, Y. 2021. Transunet: Transformers make strong encoders for medical image segmentation. *arXiv preprint arXiv:2102.04306*.
- Chen, T.; Kornblith, S.; Norouzi, M.; and Hinton, G. 2020. A simple framework for contrastive learning of visual representations. In *International conference on machine learning*, 1597–1607. PMLR.
- Chen, X.; Ding, M.; Wang, X.; Xin, Y.; Mo, S.; Wang, Y.; Han, S.; Luo, P.; Zeng, G.; and Wang, J. 2024. Context autoencoder for self-supervised representation learning. *International Journal of Computer Vision*, 132(1): 208–223.
- Chen, X.; and He, K. 2021. Exploring simple siamese representation learning. In *Proceedings of the IEEE/CVF conference on computer vision and pattern recognition*, 15750–15758.
- Dao, T.; and Gu, A. 2024. Transformers are SSMs: Generalized models and efficient algorithms through structured state space duality. In *International conference on machine learning*. PMLR.
- Devlin, J.; Chang, M.-W.; Lee, K.; and Toutanova, K. 2018. Bert: Pre-training of deep bidirectional transformers for language understanding. *arXiv preprint arXiv:1810.04805*.
- Dosovitskiy, A.; Beyer, L.; Kolesnikov, A.; Weissenborn, D.; Zhai, X.; Unterthiner, T.; Dehghani, M.; Minderer, M.; Heigold, G.; Gelly, S.; et al. 2020. An image is worth 16x16 words: Transformers for image recognition at scale. *arXiv preprint arXiv:2010.11929*.
- Goncharov, M.; Soboleva, V.; Kurmukov, A.; Pisov, M.; and Belyaev, M. 2023. vox2vec: A framework for self-supervised contrastive learning of voxel-level representations in medical images. In *International Conference on Medical Image Computing and Computer-Assisted Intervention*, 605–614. Springer.
- Grill, J.-B.; Strub, F.; Altché, F.; Tallec, C.; Richemond, P.; Buchatskaya, E.; Doersch, C.; Avila Pires, B.; Guo, Z.; Gheshlaghi Azar, M.; et al. 2020. Bootstrap your own latent—a new approach to self-supervised learning. *Advances in neural information processing systems*, 33: 21271–21284.
- Gu, A.; and Dao, T. 2023. Mamba: Linear-time sequence modeling with selective state spaces. *arXiv preprint arXiv:2312.00752*.
- Gu, A.; Goel, K.; and Ré, C. 2021. Efficiently modeling long sequences with structured state spaces. *arXiv preprint arXiv:2111.00396*.
- Hatamizadeh, A.; Tang, Y.; Nath, V.; Yang, D.; Myronenko, A.; Landman, B.; Roth, H. R.; and Xu, D. 2022. Unetr: Transformers for 3d medical image segmentation. In *Proceedings of the IEEE/CVF winter conference on applications of computer vision*, 574–584.
- He, K.; Chen, X.; Xie, S.; Li, Y.; Dollár, P.; and Girshick, R. 2022. Masked autoencoders are scalable vision learners. In *Proceedings of the IEEE/CVF conference on computer vision and pattern recognition*, 16000–16009.
- He, K.; Fan, H.; Wu, Y.; Xie, S.; and Girshick, R. 2020. Momentum contrast for unsupervised visual representation learning. In *Proceedings of the IEEE/CVF conference on computer vision and pattern recognition*, 9729–9738.
- Landman, B.; Xu, Z.; Igelsias, J.; Styner, M.; Langerak, T.; and Klein, A. 2015. Miccai multi-atlas labeling beyond the cranial vault—workshop and challenge. In *Proc. MICCAI Multi-Atlas Labeling Beyond Cranial Vault—Workshop Challenge*, volume 5, 12.
- Lay, N.; Birkbeck, N.; Zhang, J.; and Zhou, S. K. 2013. Rapid multi-organ segmentation using context integration and discriminative models. In *International Conference on Information Processing in Medical Imaging*, 450–462. Springer, Berlin, Heidelberg.
- Liu, J.; Yang, H.; Zhou, H.-Y.; Xi, Y.; Yu, L.; Yu, Y.; Liang, Y.; Shi, G.; Zhang, S.; Zheng, H.; et al. 2024. Swin-umamba: Mamba-based unet with imagenet-based pretraining. *arXiv preprint arXiv:2402.03302*.
- Liu, X.; Zhang, C.; and Zhang, L. 2024. Vision Mamba: A Comprehensive Survey and Taxonomy. *arXiv preprint arXiv:2405.04404*.
- Ma, J.; Li, F.; and Wang, B. 2024. U-mamba: Enhancing long-range dependency for biomedical image segmentation. *arXiv preprint arXiv:2401.04722*.
- Pathak, D.; Krahenbuhl, P.; Donahue, J.; Darrell, T.; and Efros, A. A. 2016. Context encoders: Feature learning by inpainting. In *Proceedings of the IEEE conference on computer vision and pattern recognition*, 2536–2544.
- Ronneberger, O.; Fischer, P.; and Brox, T. 2015. U-net: Convolutional networks for biomedical image segmentation. In *Medical image computing and computer-assisted intervention—MICCAI 2015: 18th international conference, Munich, Germany, October 5-9, 2015, proceedings, part III 18*, 234–241. Springer.
- Roy, S.; Koehler, G.; Ulrich, C.; Baumgartner, M.; Petersen, J.; Isensee, F.; Jaeger, P. F.; and Maier-Hein, K. H. 2023.

- Mednext: transformer-driven scaling of convnets for medical image segmentation. In *International Conference on Medical Image Computing and Computer-Assisted Intervention*, 405–415. Springer.
- Ruan, J.; and Xiang, S. 2024. Vm-unet: Vision mamba unet for medical image segmentation. *arXiv preprint arXiv:2402.02491*.
- Tang, F.; Nian, B.; Ding, J.; Quan, Q.; Yang, J.; Liu, W.; and Zhou, S. K. 2023. MobileUtr: Revisiting the relationship between light-weight CNN and Transformer for efficient medical image segmentation. *arXiv preprint arXiv:2312.01740*.
- Tang, Y.; Yang, D.; Li, W.; Roth, H. R.; Landman, B.; Xu, D.; Nath, V.; and Hatamizadeh, A. 2022. Self-supervised pre-training of swin transformers for 3d medical image analysis. In *Proceedings of the IEEE/CVF conference on computer vision and pattern recognition*, 20730–20740.
- Tian, K.; Jiang, Y.; Diao, Q.; Lin, C.; Wang, L.; and Yuan, Z. 2023. Designing bert for convolutional networks: Sparse and hierarchical masked modeling. *arXiv preprint arXiv:2301.03580*.
- Vaswani, A.; Shazeer, N.; Parmar, N.; Uszkoreit, J.; Jones, L.; Gomez, A. N.; Kaiser, Ł.; and Polosukhin, I. 2017. Attention is all you need. *Advances in neural information processing systems*, 30.
- Wenxuan, W.; Chen, C.; Meng, D.; Hong, Y.; Sen, Z.; and Jiangyun, L. 2021. Transbts: Multimodal brain tumor segmentation using transformer. In *International Conference on Medical Image Computing and Computer-Assisted Intervention*, Springer, 109–119.
- Woo, S.; Debnath, S.; Hu, R.; Chen, X.; Liu, Z.; Kweon, I. S.; and Xie, S. 2023. Convnext v2: Co-designing and scaling convnets with masked autoencoders. In *Proceedings of the IEEE/CVF Conference on Computer Vision and Pattern Recognition*, 16133–16142.
- Xie, Z.; Zhang, Z.; Cao, Y.; Lin, Y.; Bao, J.; Yao, Z.; Dai, Q.; and Hu, H. 2022. Simmim: A simple framework for masked image modeling. In *Proceedings of the IEEE/CVF conference on computer vision and pattern recognition*, 9653–9663.
- Xing, Z.; Ye, T.; Yang, Y.; Liu, G.; and Zhu, L. 2024. Segmamba: Long-range sequential modeling mamba for 3d medical image segmentation. *arXiv preprint arXiv:2401.13560*.
- Zhang, C.; Zheng, H.; and Gu, Y. 2023. Dive into the details of self-supervised learning for medical image analysis. *Medical Image Analysis*, 89: 102879.
- Zhou, J.; Jiang, M.; Wu, J.; Zhu, J.; Wang, Z.; and Jin, Y. 2024. MGI: Multimodal Contrastive pre-training of Genomic and Medical Imaging. *arXiv preprint arXiv:2406.00631*.
- Zhou, J.; Wei, C.; Wang, H.; Shen, W.; Xie, C.; Yuille, A.; and Kong, T. 2021. ibot: Image bert pre-training with online tokenizer. *arXiv preprint arXiv:2111.07832*.
- Zhou, Z.; Sodha, V.; Rahman Siddiquee, M. M.; Feng, R.; Tajbakhsh, N.; Gotway, M. B.; and Liang, J. 2019. Models genesis: Generic autodidactic models for 3d medical image analysis. In *Medical Image Computing and Computer Assisted Intervention—MICCAI 2019: 22nd International Conference, Shenzhen, China, October 13–17, 2019, Proceedings, Part IV 22*, 384–393. Springer.
- Zhu, L.; Liao, B.; Zhang, Q.; Wang, X.; Liu, W.; and Wang, X. 2024. Vision mamba: Efficient visual representation learning with bidirectional state space model. In *International conference on machine learning*. PMLR.

6 Appendix

6.1 The Proof for Selective Structure State Space Sequence Token-interpolation (S6T)

Structured State Space Sequence Models (S4) and Mamba, both rely on a classical continuous system that maps a one-dimensional input function or sequence, denoted as $x(t) \subseteq R$, through intermediate implicit states $h(t) \subseteq R^N$ to an output $\hat{y}(t) \subseteq R$

Theorem 1. $A' \subseteq R^{N \times N}$ represents the state matrix, $B' \subseteq R^{N \times 1}$ and $C' \subseteq R^{N \times 1}$ denote the projection parameters. S4 can be written as:

$$\begin{aligned} h'(t) &= A'h(t) + B'x(t) \\ \hat{y}(t) &= C'h(t) \end{aligned} \quad (9)$$

From theorem.1, we can see that this is the basic state equation, where A' , B' , and C' are unknown parameters which needed to be pre-setted.

We are now considering the reverse scenario. If we have a set of $h'(t)$, $x(t)$, and $\hat{y}(t)$, Can we determine the values of A' , B' , and C' ? In theory, we have the capability to solve for the values of A' , B' , and C' . However, this might be computationally infeasible for a computer to solve. So, we choose to reduce the number of unknown parameters and retain only the most important one. We can get a corollary about state space model.

Corollary 1.1. Let B' And C' are setted as identify martix. And the S4 can be rewritten as :

$$\begin{aligned} h'(t) &= A'h(t) + x(t) \\ \hat{y}(t) &= h(t) \end{aligned} \quad (10)$$

Now, we need to solve Equation.12. As Eq.11, if we directly integrate A, then h(t) cannot be determined with continuous-time t.

$$h'(t) = A'h(t) + x(t) = h(t) = h(0) + \int_0^t (A'h(\delta) + x(\delta))d\delta \quad (11)$$

So we need to change our approach to deduce a method that eliminates the integration of $h(t)$.

Lemma 2. Given timesacle Δ , the discretized Equation.12 can be writted as:

$$\begin{aligned} h'(t) &= A'h(t) + x(t) \\ \hat{y}(t) &= h(t) \\ A' &= e^{\Delta A'} \\ B &= (e^{\Delta A'} - I)\Delta A'^{-1} \end{aligned} \quad (12)$$

Proof. Here we choose to construct a new function $\alpha(t)h(t)$ for $h(t)$.

- $\alpha(t)h(t)$
- $\frac{d}{dt}[\alpha(t)h(t)] = \alpha(t)h'(t) + \frac{d\alpha(t)}{dt}x(t)$
- $\frac{d}{dt}[\alpha(t)h(t)] = \alpha(t)(A'h(t) + x(t)) + \frac{d\alpha(t)}{dt}h(t)$
- $\frac{d}{dt}[\alpha(t)h(t)] = (A'\alpha(t) + \frac{d\alpha(t)}{dt})h(t) + \alpha(t)x(t)$

- To eliminate $h(t)$, we need to make its coefficients equals zero
- $A'\alpha(t) + \frac{d\alpha(t)}{dt} = 0$
- We can see that this is a first-order ordinary differential equation. And we can get solution.
- $\alpha(t) = e^{-A't}$, $\frac{d}{dt}[\alpha(t)h(t)] = \alpha(t)x(t)$
- $e^{-A't}h(t) = h(t) + \int_0^t e^{-A'\delta}x(\delta)d\delta$
- $e^{A't}e^{-A't}h(t) = e^{A't}h(t) + e^{A't}\int_0^t e^{-A'\delta}x(\delta)d\delta$
- $h(t) = e^{A't}h(0) + \int_0^t e^{A'(t-\delta)}x(\delta)d\delta$
- Consider the sampling time instant t_k, t_{k+1} and $T = t_{k+1} - t_k$
- $h(t_{k+1}) = e^{A't_{k+1}}h(0) + \int_0^{t_{k+1}} e^{A'(t_{k+1}-\delta)}x(\delta)d\delta$,
 $h(t_k)e^{A't_k}h(0) + \int_0^{t_k} e^{A'(t_k-\delta)}x(\delta)d\delta$
 $= [e^{A(t_{k+1}-t_k)}][e^{A t_k}h(0) + \int_0^{t_k} e^{A(t_k-\delta)}x(\delta)d\delta]$
 $+ \int_{t_k}^{t_{k+1}} e^{A(t_{k+1}-\delta)}x(\delta)d\delta$
- $h_{k+1} = e^{A't_{k+1}-t_k}x(t_k) + \int_0^{t_k} e^{A'(t_k-\delta)}x(\delta)d\delta$
 $+ \int_{t_k}^{t_{k+1}} e^{A'(t_{k+1}-\delta)}x(\delta)d\delta$
- consider $h(t)$ in time $t_k - t_{k+1}$ unchanged.
- $h(t) = e^{A'T}x(t_k) + x(t_k)\int_{t_k}^{t_{k+1}} e^{A'(t_{k+1}-\delta)}d\delta$
- $\int_0^T e^{A'\delta} = A'^{-1}(e^{A'T} - I)$
- now we can get equation of $x(t_{k+1})$
- $x_{t_{k+1}} = e^{A'T}x_{t_k} + (e^{A'T} - I)A'^{-1}x(t_k)$
- $A' = e^{\Delta A'}, B = (e^{\Delta A'} - I)\Delta A'^{-1}$

□

we can see that in fact, B' is also composed by A' . Now we will also consider deep learning and utilize its characteristics for further simplification. A' will be randomly generated and continuously iterated, which is a dynamic process in Token-interpretation.

As for B' , consider $B' = e^{\Delta A'}\Delta A'^{-1} - \Delta A'^{-1} \approx e^{\Delta A'}A'^{-1}$, The quation can be written further as :

$$\begin{aligned} \bar{K} &= (e^{\Delta A'}\Delta A'^{-1}, e^{2\Delta A'}\Delta A'^{-1}, \dots, e^{(L-1)\Delta A'}\Delta A'^{-1}) \\ \hat{y} &= x * \bar{K} \end{aligned} \quad (13)$$

where $\bar{K} \in R^L$ represents a structure convolutional kernel, and L is the length of input sequence x.

Lemma 3. Let $\hat{y} = [\hat{y}_i = z_0, z_1, z_2, \dots, z_{Q+2}, \hat{y}_{i+1}]$, $\bar{A} = e^{\Delta A}$, we can get the expression of S6T:

$$\begin{aligned} z_i &= \sum_{n=0}^i (\bar{A}'^{i-n}\Delta A'^{-1}) \cdot s'_n \\ s'_n &= \frac{Q+2-n}{Q+2} \cdot \hat{y}_i + \frac{n}{Q+2} \cdot \hat{y}_{i+1} \\ \bar{A}' &= e^{\Delta A'} \end{aligned} \quad (14)$$